JOURNAL OF GEOPHYSICAL RESEARCH, VOL. 114, D13205, doi:10.1029/2008JD011115, 2009

Aerosol analysis and forecast in the European Centre for Medium-Range Weather Forecasts Integrated Forecast System: 2. Data assimilation

A. Benedetti,[1] J.-J. Morcrette,[1] O. Boucher,[2] A. Dethof,[1] R. J. Engelen,[1] M. Fisher,[1] H. Flentje,[3] N. Huneeus,[4] L. Jones,[1] J. W. Kaiser,[1] S. Kinne,[5] A. Mangold,[6] M. Razinger,[1] A. J. Simmons,[1] and M. Suttie[1]

Received 5 September 2008; revised 30 April 2009; accepted 6 May 2009; published 11 July 2009.

[1] This study presents the new aerosol assimilation system, developed at the European Centre for Medium-Range Weather Forecasts, for the Global and regional Earth-system Monitoring using Satellite and in-situ data (GEMS) project. The aerosol modeling and analysis system is fully integrated in the operational four-dimensional assimilation apparatus. Its purpose is to produce aerosol forecasts and reanalyses of aerosol fields using optical depth data from satellite sensors. This paper is the second of a series which describes the GEMS aerosol effort. It focuses on the theoretical architecture and practical implementation of the aerosol assimilation system. It also provides a discussion of the background errors and observations errors for the aerosol fields, and presents a subset of results from the 2-year reanalysis which has been run for 2003 and 2004 using data from the Moderate Resolution Imaging Spectroradiometer on the Aqua and Terra satellites. Independent data sets are used to show that despite some compromises that have been made for feasibility reasons in regards to the choice of control variable and error characteristics, the analysis is very skillful in drawing to the observations and in improving the forecasts of aerosol optical depth.

Citation: Benedetti, A., et al. (2009), Aerosol analysis and forecast in the European Centre for Medium-Range Weather Forecasts Integrated Forecast System: 2. Data assimilation, *J. Geophys. Res.*, *114*, D13205, doi:10.1029/2008JD011115.

1. Introduction

[2] Environmental monitoring is a fundamental activity given the current rapid transformations of the natural environment due to human activity. In particular, monitoring of greenhouse gases, reactive gases and atmospheric particulate plays an important role due to the open-ended debate about climate change and its long-term implications [*Bellouin et al.*, 2008]. Issues raised by the proven links between some atmospheric constituents, such as ozone and particulate, and human health have also raised the level of attention toward these activities [*Thompson et al.*, 2006; *Lewtas*, 2007].

[3] One of the foremost projects dedicated to this goal is the Global and regional Earth-system (Atmosphere) Monitoring using Satellite and in-situ data (GEMS) project, which counts 32 European partners with expertise in various aspects of atmospheric composition monitoring. GEMS is part of the Global Monitoring for Environment and Security (GMES) initiative and was established under European Commission funding in 2005 to create an assimilation and forecasting system for monitoring aerosols, greenhouse gases and reactive gases, at global and regional scales, through exploitation of satellite and in situ data [*Hollingsworth et al.*, 2008]. An important component of GEMS is also monitoring of regional air quality at the European scale which is performed with an ensemble of models from the participating institutes. Boundary conditions for the high-resolution models are provided by the global model.

[4] Forecast and analysis systems for atmospheric constituents have been developed. The basis for these schemes is the operational ECMWF Integrated Forecasting System (IFS) and the incremental four-dimensional variational analysis system. These systems have been extended to include new prognostic variables for atmospheric tracers (i.e., gases and aerosols). A coupled chemical transport model is also part of the GEMS system and provides tendencies for the chemically active species which are present in the model. In this paper, we will focus on the development and the performance of the aerosol analysis system. Companion papers by *Morcrette et al.* [2008] (hereafter, part 1) and by A. Mangold et al. (Aerosol analysis and forecast in the European Centre for Medium-

[1]European Centre for Medium-Range Weather Forecasts, Reading, UK.
[2]Met Office, Exeter, UK.
[3]Meteorologisches Observatorium Hohenpeissenberg, Deutscher Wetterdienst, Hohenpeissenberg, Germany.
[4]Laboratoire des Sciences du Climat et de l'Environnement, Gif-sur-Yvette, France.
[5]Max-Planck-Institut für Meteorologie, Hamburg, Germany.
[6]Observations Department, Royal Meteorological Institute of Belgium, Uccle, Belgium.

0148-0227/09/2008JD011115$09.00

Range Weather Forecasts Integrated Forecast System: 3. Evaluation, manuscript in preparation, 2008) (hereafter, part 3) discuss in detail the aerosol model and the validation of the forecast/analysis results, respectively.

[5] Modeling and prediction of aerosols is associated with a large degree of uncertainty due to uncertainties in the emissions, transport and nonlinear physical processes involving aerosols (for example, radiative effects, cloud and rain formation). Ground-based observing networks have been crucial in improving our knowledge of this atmospheric component, complemented in more recent years by satellite sensors which offer a more global view of the aerosol distribution. Harmonization of models and data is, however, required in order to tackle the model deficiencies and to obtain a more accurate representation of aerosols and their interaction with the atmospheric system as a whole.

[6] The current attempt at variational data assimilation of satellite aerosol data into a global Numerical Weather Prediction (NWP) model for reanalyses and forecasts is an unprecedented effort. Previous applications in this relatively young field, aimed at assimilating aerosol in global models use the Optimal Interpolation approach, and focused on regional studies [*Collins et al.*, 2001; *Rasch et al.*, 2001]. A global assimilation OI system is described by *Generoso et al.* [2007] and was used to better constrain the Arctic aerosol burden. *Weaver et al.* [2007] describe an off-line retrieval/assimilation system for the Goddard Chemistry and Aerosol Radiation Transport (GOCART) model using Moderate Resolution Imaging Spectroradiometer (MODIS) radiances based on the Kalman filter approach. Successful four-dimensional variational (4D-Var) aerosol assimilation has been implemented in a chemical transport model by *Fonteyn et al.* [2000] and *Errera and Fonteyn* [2001]. More recently, *Zhang et al.* [2008] described the first attempt at building a 3D-Var system for operational aerosol assimilation using the Naval Research Laboratory (NRL) model, while *Niu et al.* [2008] introduced a novel data assimilation system for dust aerosols in the Chinese Unified Atmospheric Chemistry Environment–Dust (CUACE/Dust) forecast system.

[7] With respect to previous studies with chemical transport models, which are often dependent on prescribed meteorological fields, the aerosol model described here is fully integrated into the forecasting model, and the assimilation scheme is part of the meteorological 4D-Var system employed operationally at ECMWF. This offers the unique advantage to have consistent and accurate meteorological fields which are constrained by the huge number of observations routinely assimilated. Fields such as winds are used in the parameterizations to describe the emissions of natural aerosols, i.e., desert dust and sea salt. The aerosol description also benefits from being integrated into state-of-the-art convection and diffusion parameterizations. Of note is also the fact that this is the first European effort at building a preoperational global system for routine aerosol assimilation and forecasting.

[8] The aerosol assimilation system has been recently completed and has been used to produce a 2-year analysis for 2003–2004. Furthermore, a version of this system is currently used for near-real-time forecasts of aerosol fields. Observations assimilated are the aerosol optical depths (AOD) retrieved from the MODIS instruments on board the Terra and Aqua satellites. The building blocks of the system are described in section 2. Section 3 presents the observations used in the reanalysis along with a discussion of biases and representativeness errors. The experimental setup is also described in section 3. Analysis biases are discussed in section 4. An example from the near-real-time experiment which started in July 2008 is presented in section 5 to show the impact of the MODIS data on the aerosol forecast. Results from the analysis for 2003 are examined in detail in section 6 with focus on the month of May 2003. A validation of these results using independent observations from the AErosol RObotic NETwork (AERONET) is also presented. It is demonstrated that the GEMS aerosol assimilation system has good potential to provide high-quality analysis and forecasts of atmospheric particulate.

2. Technical Description of the Aerosol Assimilation System

2.1. Aerosol Model

[9] The implementation of an aerosol module in the ECMWF model has involved the introduction of new prognostic variables (i.e., aerosol mass mixing ratios) and the definition of aerosol-specific physical parameterizations (see part 1). The physical package for aerosols was partially taken from the Laboratoire d'Optique Atmosphérique (LOA) Laboratoire de Météorologie Dynamique (LMD) model [*Boucher et al.*, 2002; *Reddy et al.*, 2005]. It includes sources for sea salt and desert dust and a representation of sedimentation, and wet and dry deposition processes. The sedimentation scheme has been modified following recent developments by *Tompkins* [2005] while the wet and dry deposition schemes were adapted directly from the LMD model. All aerosol species are treated as tracers in the IFS vertical diffusion and convection schemes and are advected by the semi-Lagrangian scheme, consistently with all other dynamical fields and tracers. Five types of tropospheric aerosols are included: sea salt, desert dust, organic matter, black carbon and sulphate aerosols. Stratospheric aerosols are not included in the current assimilation configuration.

[10] Aerosols of natural origin such as sea salt and desert dust are represented via a three-bin formulation. Bin limits for sea salt are set at 0.03, 0.5, 5 and 20 μm and for desert dust at 0.03, 0.55 0.9 and 20 μm. This ensures that approximately 10, 20 and 70% of the total mass is included in the three respective bins. For organic matter and black carbon both the hydrophobic and the hydrophilic component are modeled. Sulphates are represented as one variable. There are no gaseous chemistry parameterizations for sulphate included in this version of the model which means that the model sulphate is only in the aerosol form. A newer version of the model which accounts for gas-to-particle conversion of SO_2 is currently being tested.

[11] State-of-the-art emission sources have been implemented and are described extensively in part 1. For anthropogenic aerosol, the sources come from available emission inventories (GFED, Global Fire Emission Database; SPEW, Speciated Particulate Emission Wizard; EDGAR, Emission Database for Global Atmospheric Research). For natural aerosol, the sources are instead related to model parameters (i.e., 10-m wind for sea salt, soil moisture and wind for

desert dust, among others). The aerosol model provides the background information to feed into the variational assimilation system described below.

2.2. ECMWF 4D-Var

[12] The variational method is a well-established approach which combines model background information with observations to obtain the "best" forecast possible. This approach is widely used in many NWPs centers. The method is based on minimization of a cost function which measures the distance between observations and their model equivalent, subject to a background constraint usually provided by the model itself. Optimization of this cost function is performed with respect to selected control variables (e.g., the initial conditions). Adjustments to these control variables allow for the updated model trajectory to match the observations more closely. Assuming the update to the initial condition (also known as the increment) is small, an incremental formulation can be adopted to ensure a good compromise between operational feasibility and physical consistency in the analysis [*Courtier et al.*, 1994]. The cost function in the incremental approach can be written as

$$J(\delta x_0) = \frac{1}{2}\delta x_0^T \mathbf{B^{-1}} \delta \mathbf{x_0} + \frac{\mathbf{1}}{\mathbf{2}} \sum_{\mathbf{i=0}}^{\mathbf{n}} \left(\mathbf{H_i'}\delta \mathbf{x_i} - \mathbf{d_i}\right)^{\mathbf{T}} \mathbf{R^{-1}} \left(\mathbf{H_i'}\delta \mathbf{x_i} - \mathbf{d_i}\right) + \mathbf{J_c}(\delta \mathbf{x_0}), \quad (1)$$

where $\delta x_i = x_i - x_i^b$ is the analysis increment and represents the departure of the model state ($\mathbf{x}$) with respect to the background ($\mathbf{x^b}$) at time t_i. H' is the linearized observation operator and $d_i = y_i^o - H_i(x_i^b)$ is the departure of the model background equivalent from the observation (y_i^o). The matrix $\mathbf{R}$ is the observation error covariance matrix, which accounts both for pure observation errors (instrumental, calibration, retrieval) and for representativeness errors due to forward model assumptions and to the interpolations needed to go from model to observation space. $\mathbf{B}$ represents the background error covariance matrix, formulated according to the "wavelet–J_b" method of M. Fisher (Background error covariance modeling, Seminar on Recent Developments in Data Assimilation for Atmosphere and Ocean, ECMWF, Reading, U. K., 2003, and Generalized frames on the sphere, with application to background error covariance modeling, paper presented at Seminar on Recent Developments in Numerical Methods for Atmospheric and Ocean Modelling, ECMWF, 2004). The aerosol-specific background error covariance matrix is discussed briefly in section 2.3 and more extensively by *Benedetti and Fisher* [2007]. The $\mathbf{R}$ and $\mathbf{B}$ matrices represent respectively the relative weight assigned to observations and background fields in the analysis. The background at $t = 0$, $\mathbf{x_0^b}$, is obtained from a short-range forecast valid at the initial time of the assimilation period. A penalty cost function, J_c ($\delta \mathbf{x_0^b}$), is used to impose other physical constraints on the solution (i.e., to filter out gravity waves).

[13] The flow of the 4D-Var minimization is as follows. A nonlinear integration provides the state in the vicinity of which the model is linearized (trajectory). For operational purposes the analysis increments are computed at a lower resolution than the forecast model integration. A stepwise procedure is applied and departures are first computed during the nonlinear integration at high resolution, then they are interpolated to the lower resolution. The gradient of the cost function required in the minimization is computed using the adjoint model.

[14] The minimization is solved using an iterative algorithm, based on the Lanczos conjugate gradient algorithm with appropriate preconditioning. In order to reduce the computational costs and strong nonlinearities in the operational 4D-Var system, the perturbations $\delta \mathbf{x}_i$ are computed with a tangent-linear model using simplified physics [*Tompkins and Janisková*, 2004; *Lopez and Moreau*, 2005] at a lower resolution than the nonlinear trajectory.

[15] After the minimization, the model trajectory and the departures are recomputed and a second minimization at a higher horizontal resolution is run. For the analysis, a resolution of T159 (corresponding to ~120 km) is used in the nonlinear trajectory and the forecast, while the two minimizations are run at T95 (~215 km) and T159. An average of 50–70 iterations is required to reach a satisfactory convergence of the minimization. Convergence criteria and a detailed description of the incremental 4D-Var is given by M. Fisher (Minimization algorithms for variational data assimilation, paper presented at Seminar on Recent Developments in Numerical Methods for Atmospheric Modelling, ECMWF, Reading, U. K., 1998) and *Trémolet* [2005].

[16] The assimilation window is 12 h. MODIS observations of aerosol optical depth together with all other meteorological data are subdivided into time slots of 30 min and ingested over the window. A thinning is applied to better match the spatial resolution of the observations to that of the analysis. A different approach may be considered which involves averaging the MODIS retrievals over the grid box. This approach would reduce the observational error but would have an associated representativeness error. As a first step we decided to follow what is done for most meteorological data in the ECMWF assimilation system, that is to interpolate the model data, including the aerosol mass mixing ratios, to the observation location after the thinning is performed. The model equivalent of the observations is then computed using the specific observation operator. The operator for AOD is described in section 2.4.

2.3. Background Error Covariance Matrix for Aerosols

[17] The aerosol $\mathbf{B}$ matrix used for the GEMS aerosol reanalysis was derived using the Parrish and Derber method (also known as NMC method [*Parrish and Derber*, 1992]) as detailed by *Benedetti and Fisher* [2007]. The difference with respect to the results presented in that paper lies in the use of updated error statistics derived from forecast differences computed with the current aerosol model described in section 2.1. The method is the following: 6 months of 2-day forecasts at T159 are run and the differences between the 48-h and the 24-h forecasts are used as statistics for the estimate of the background errors. These are in turn used to construct a B matrix using the wavelet technique devised by *Fisher* [2006] (see also Fisher, presented paper, 2003).

[18] The difference between the old and the revisited sets of statistics is mainly seen in the significantly smaller standard deviation of the latter, reflecting the fact that the current model has a smaller degree of variability between

Table 1. Optical Properties at 550 nm and 50% Relative Humidity

Aerosol Type	α_e (m^2 g^{-1})	ω	g
Sulphate	6.609	1.000	0.673
Black carbon	9.412	0.206	0.335
Organic matter	5.502	0.982	0.655
Dust			
0.03–0.55 μm	2.6321	0.9896	0.7300
0.55–0.9 μm	0.8679	0.9672	0.5912
0.9–20.0 μm	0.4274	0.9441	0.7788
Sea salt			
0.03–0.5 μm	3.0471	0.9996	0.7394
0.5–5.0 μm	0.3279	0.9961	0.7703
5.0–20.0 μm	0.0924	0.9916	0.8224

the aerosol forecasts at 24 and 48-h with respect to the previous version. This, in turn, translates into a smaller background error, which is more realistic given the improvements implemented in the current version of the aerosol model. With this new lower background error, the analysis, while still drawing to the observations, relies more on the model background constraint since the relative weight between the background and the observations is decided by the error statistics prescribed for both. This is extremely important, especially in areas that are data-limited such as the polar regions where the aerosol analysis is severely underconstrained relative to the observations and relies almost entirely on the background. More details on the impact of the different sets of statistics on the analysis are presented by *Benedetti et al.* [2008].

[19] *Benedetti and Fisher* [2007] showed that the NMC method leads to a satisfactory background error covariance matrix without the need to prescribe the vertical and horizontal correlation lengths. The NMC method applied to the definition of background error statistics for aerosol has also been revisited and compared with other methods by *Kahnert* [2008], who concluded that it is the most appropriate for assimilation over the time windows typically used in NWP applications (6–12 h).

2.4. Observation Operator

[20] The observation operator for aerosol optical depth is based on precomputed optical properties (mass extinction coefficient, α_e, single scattering albedo, ω, and asymmetry parameter, g) for the relevant aerosol species included in the model. The aerosols are assumed to be externally mixed. That is, the individual species are assumed to coexist in the volume of air considered and to retain their individual optical and chemical characteristics. While this is might be a limitation as most aerosol in nature are internally mixed, it makes the problem more tractable in the context of a numerical forecast model. The optical characteristics of the aerosols are computed at the MODIS wavelengths using Mie theory (i.e., particles are assumed to be spherical in shape), and integrated over the physical size range using a prescribed lognormal distribution following *Reddy et al.* [2005]. The fixed parameters in the distribution are the mode radius and the standard deviation, and these vary from species to species. The assumed values are reported in Table 2 of *Reddy et al.* [2005]. Optical properties of hygroscopic aerosols such as sulphate, hydrophilic organic matter and sea salt, are parameterized as a function of relative humidity (RH). Table 1 summarizes the optical properties at 550 nm and 50% RH.

[21] For the calculation of the model equivalent optical depth, the relative humidity is first computed from the model temperature, pressure and specific humidity. The appropriate mass extinction coefficients are then retrieved from the look-up table for the wavelength of interest (here, 550 nm), multiplied by the aerosol mass which has been previously interpolated at the observation locations, and then integrated vertically. The total optical depth is the sum of the single-species optical depths as given by

$$\tau_\lambda = \sum_{i=1}^{N} \int_{p_{surf}}^{0} \alpha_{ei}(\lambda, RH(p)) r_i(p) \frac{dp}{g}, \qquad (2)$$

where N is the total number of aerosol species, r is the mass mixing ratio, dp is the pressure of the model layer and g is the constant of gravity; p_{surf} represents the surface pressure.

2.5. Total Aerosol Mixing Ratio as Control Variable

[22] The aerosol model comprises a mixed bin and bulk representation of the aerosol species. This was deemed to be a necessary compromise between a full-blown bin representation of all species which would have introduced many more tracers in the IFS, and a modal representation of the aerosols which would possibly have oversimplified the aerosol model. However, the eleven additional tracers that are currently used in the forward model, can constitute a heavy burden for the analysis if they are all included in the control vector. The reason for this is threefold: (1) background error statistics would have to be generated for all species separately, (2) the control vector would be much larger in size which would, in turn, increase the cost of the iterative minimization, and most importantly, (3) the aerosol analysis would be severely underconstrained as one observation of total aerosol optical depth would be used to constrain eleven profiles of aerosol species. As a way to alleviate these problems, the total aerosol mixing ratio, defined as the sum of the eleven aerosol species, is used instead as control variable. At each iteration of the minimization, the increments in the total mixing ratio deriving from the assimilation of MODIS optical depths have to be redistributed into the mixing ratios of the single species. Even with this expedient, the problem remains underconstrained with respect to the observations, and the redistribution of the increments relies heavily on the background. However, the size of the control vector is more manageable. Some assumptions are needed in order to implement this control variable correctly: (1) The sum of the single species has to be equal to the total mixing ratio at all times and for all locations; that is, the aerosol mass needs to be conserved over the 12-h assimilation window. (2) The relative contribution of a single species/bin to the total mixing ratio has to be kept constant over the assimilation window.

[23] Assumption 1 implies that processes which do not conserve the aerosol mass, such as deposition and sedimentation, should not be activated during the trajectory run. Assumption 2 follows from assumption 1, and effectively implies that perturbations from species with higher specific density contribute more to the perturbation in total mixing

ratio even if their contribution to the optical thickness at a given wavelength might be smaller than that of species with lower specific density. It is worth emphasizing that the total aerosol mixing ratio is introduced as a prognostic variable that undergoes all advective and diffusive processes and is initialized from the sum of the single mixing ratios. However, it is only a control variable and not a "real" physical variable. If there are nonconservative processes it cannot be assumed that the total mixing ratio which has been advected and diffused is equal to the sum of the individual species at every grid point and time step over the assimilation window, during the minimization. However, if the removal processes can be assumed to be slower with respect to advection and diffusion, then in first approximation the prognostic total mixing ratio truly represents the sum of all mixing ratios. In practice the above-stated assumptions are relaxed and the trajectory run is performed with all aerosol processes switched on. This still provides a meaningful analysis since most of the dominant physical processes happen over time scales longer than 12 h. For example, the typical residence time for the largest bin of desert dust and sea salt is approximately 1 day, whereas anthropogenic species have a typical residence time of a week.

[24] The way this control variable works is the following. In the nonlinear trajectory run the total aerosol mixing ratio is computed by summing all species/bins; that is, $r_T = \sum_{i=1}^{N} r_i$, where r is the mixing ratio, and the subscript T indicates the total mixing ratio. All aerosol variables, including the total aerosol mixing ratio, are subject to advection, vertical diffusion and convection. The mixing ratios of the individual species are used to compute the total optical depth using the tabulated optical properties as outlined in section 2.4. The tangent linear run is then started with zero perturbations for the single species to compute the perturbation in optical depth. The latter is passed to the adjoint routine to compute the gradient with respect to the individual species. The gradient with respect to the total mixing ratio is obtained as

$$r_T^* = \sum_{i=1}^{N} f_i r_i^*, \tag{3}$$

where r_i^* is gradient of the mixing ratio and $f_i = (\frac{r_i}{r_T})$ is the fractional contribution of the single species to the total mass. The gradient with respect to the total mixing ratio is then used in the minimization and the resulting increment in r_T' is used in the following iteration of the tangent linear run to compute updated perturbations r_i' on the individual species/bin mixing ratios as follows:

$$r_i' = f_i r_T'. \tag{4}$$

These, in turn, are used to compute perturbations in optical depth to be fed to the adjoint, and so on until the convergence criteria is met. To avoid the analyzed total aerosol mixing ratio becoming negative as a result of adding a negative increment, the total aerosol mixing ratio is screened for values less than zero and reset to zero when those happen.

3. Data Description and Experimental Setup

3.1. MODIS Aerosol Retrievals

[25] Of the available satellite data sources for aerosol optical depth data, the MODIS instrument on board of Terra and Aqua was selected for its reliability. The availability of data in near real time was a further factor. These are important aspects in view of an envisaged operational application. The retrievals of aerosol optical depth from MODIS are described by *Remer et al.* [2005]. Two separate retrievals with different accuracies are applied over land and ocean. The retrievals over land suffer from higher uncertainties due to the impact of the surface reflectance. Over highly reflective surfaces, such as deserts and snow-covered areas, there is not sufficient contrast to discern the aerosol signal from the surface signal. For this reason, the land retrieval is only possible over "dark" surfaces. Several other factors affect the accuracy of the retrievals both over land and ocean: cloud contamination, assumptions about the aerosol types and size distribution, near-surface wind speed, radiative transfer biases, and instrumental uncertainties. These factors are reviewed in detail by *Zhang and Reid* [2006].

[26] For our purposes the most recent MODIS release (collection 5) was used since it has been proven to be more accurate, particularly over land. MODIS retrieved optical depths are provided at different wavelengths. These are 470 nm, 550 nm, 660 nm, 870 nm, 1240 nm, 1630 nm and 2130 nm. However, as a first step, only the optical depth at 550 nm is assimilated in the analysis. In what follows it is understood that aerosol optical depth refers to the aerosol optical depth at a wavelength of 550 nm, unless otherwise stated.

[27] The original MODIS retrievals have a resolution of 10×10 km. Since the analysis is run at T159 which is approximately 120×120 km, the MODIS optical depths are thinned to this coarser resolution. Observations are taken at the original location and model aerosol fields are interpolated to this location before applying the observation operator described in section 2.4.

3.2. Discussion of Observations and Model Biases

[28] Observation and model biases are very important to characterize for a successful analysis, as the analysis itself does not remove biases, but only aims at minimizing the error between model and observations in a least square sense. *Zhang and Reid* [2006] propose a method to remove biases from the MODIS ocean aerosol product before assimilation in the NRL system through quality assurance procedures and selective data screening. They indicate that the reduction in error between the corrected MODIS and the AERONET verifying data can be 10–20%, mainly owing to the elimination of the cloud-contaminated retrievals. While recognizing the validity of this effort we did not apply a similar rigorous procedure to the MODIS data. Our initial approach was instead to devise a correction dependent on the model optical depth as described by *Benedetti and Janisková* [2008] for the assimilation of MODIS cloud optical depths. In that study, the authors divide the range

of possible optical depths into eighteen bins and for each bin they calculate the average of the corresponding first-guess departures. The averages are then stored and subsequently subtracted during the assimilation run from the model optical depths falling in the specific bin. One of the shortcomings of this method is that model biases can be aliased into observation biases. We applied this procedure to the aerosol analysis, choosing an optical depth range between 0 and 5 for the binning procedure. It was found that, for aerosol optical depth this bias correction does not improve the analysis. This is possibly because checks based on first-guess departures do not flag cases in which both the observations and the first guess have large biases, but the difference between the two is small [*Zhang et al.*, 2008]. It was hence decided not to implement any bias correction. All results presented here are from an analysis with the raw MODIS optical depth data. The issue of a bias correction for the MODIS aerosol retrievals is still open and will be addressed in the future. Different alternatives will be explored, such as using existing bias-corrected data sets such as that of *Zhang and Reid* [2006] or using in-house tools. In particular, we see the potential of applying an online correction which is estimated as part of the 4D-Var minimization, following the work of *Dee* [2005].

3.3. Observation and Representativeness Errors

[29] The overall uncertainty of the MODIS aerosol optical depth product is given by *Remer et al.* [2005]. The ocean retrievals are shown to be more accurate than the land retrievals with an estimated uncertainty $\Delta\tau = \pm 0.03 \pm 0.05\,\tau$. Land retrievals are assigned a $\Delta\tau = \pm 0.05 \pm 0.15\,\tau$. The authors also quote a relative error between the MODIS land retrievals and AERONET observations of 41% at 0.55 μm where MODIS shows a positive bias and overestimates τ.

[30] In this study the error on over-ocean retrievals of aerosol optical depth at 0.55 μm was reassigned following B. Crouzille et al. (Methodology for quality assurance MODIS aerosol products, 2007, ECMWF, available at http://gems.ecmwf.int). In their study the authors analyze the MODIS retrievals to devise a multiregression formula for assigning errors as a function of the scattering angle at a pixel level. They make use of the quality flags provided as part of the standard MODIS product, to choose and include only "good" retrievals in the regression. Following their analysis, the standard deviation of the aerosol product over ocean, ϵ_{τ_o} can be parameterized as

$$\epsilon_{\tau_o} = \max(0.05, \tau_o(a + b * \Theta) + c), \tag{5}$$

where $a = 0.007$, $b = 0.0012$ and $c = 0.001$ are the regression coefficients, τ_o is the aerosol optical depth over ocean, and Θ is the scattering angle. In the current study a slightly different formulation was used. As it was noticed that the free-running forecast tends to overpredict optical depth over the oceans as discussed in part 1, the minimum error for the MODIS product was taken to be 0.02 according to the following formula:

$$\epsilon_{\tau_o} = \max(0.02, \tau_o(a + b * \Theta) + c) \tag{6}$$

in order to bind the analysis more to the observations. An extra five percent error was arbitrarily added to account for errors due to the interpolation of the aerosol fields to the observation location (representativeness error).

[31] For the land retrievals, it was decided to assign an arbitrarily inflated error to account for the discrepancies with the AERONET product also mentioned by *Remer et al.* [2005] and representativeness. The error for land retrievals, ϵ_{τ_l}, was hence assigned as

$$\epsilon_{\tau_l} = \max(0.02, 0.5\tau_l) \tag{7}$$

where τ_l is the aerosol optical depth over land. The impact of these choices for the errors are discussed in section 4.

[32] Other sources of representativeness error for aerosol optical depth, not included in the current formulation, are discussed by *Tsigaridis et al.* [2008]. Those are related to the assumptions made on the underlying aerosol model which is used to obtain the optical properties, for example the assumption of sphericity of the aerosol particles, the choice of the size distribution and its parameters (characteristic radius and variance) the preassigned hygroscopic behavior of the aerosols, and most importantly the assumption on the state of mixing of the aerosol particulate, most commonly treated as comprising individual noninteracting chemical species (external mixtures). All these can contribute to increase the error on the optical depth by up to 30%. In the future there will be an attempt to include these uncertainties into the assignment of the observation error, but in the current study these error contributions were neglected.

3.4. Experimental Setup

[33] All reanalysis tests and the long reanalyses were run with the same configuration. Species included in the analysis are sea salt, desert dust, black carbon, organic matter and sulphate. It was decided not to include stratospheric aerosol because of the low concentrations for the years 2003–2004. The model resolution was set to T159 and 60 vertical levels. The background error covariance matrix was specified as detailed in section 2.3, while the observation covariance matrix was assumed to be diagonal with standard deviations prescribed by equations (6) and (7). The setup for the near-real-time experiment is in everything identical to that for the analysis with the only difference that the forecast is run up to 72 h instead of 24 h.

[34] Initial tests covered a period of ten days in April 2003 and were used to look at the general behavior of the analysis. The month of May 2003 was used for more extensive statistics on the analysis biases. Lessons learned from this investigation are discussed in the section below.

4. Analysis Biases

[35] The aerosol optical depth from the analysis for the whole month of May 2003 was used to investigate the analysis performance with respect to the assimilated observations. This type of comparison is considered a sanity check. In a successful analysis the departures should always be smaller than the first-guess departures, and the analysis should match the observations better in a statistical sense. Figure 1 shows scatterplots of assimilated aerosol observa-

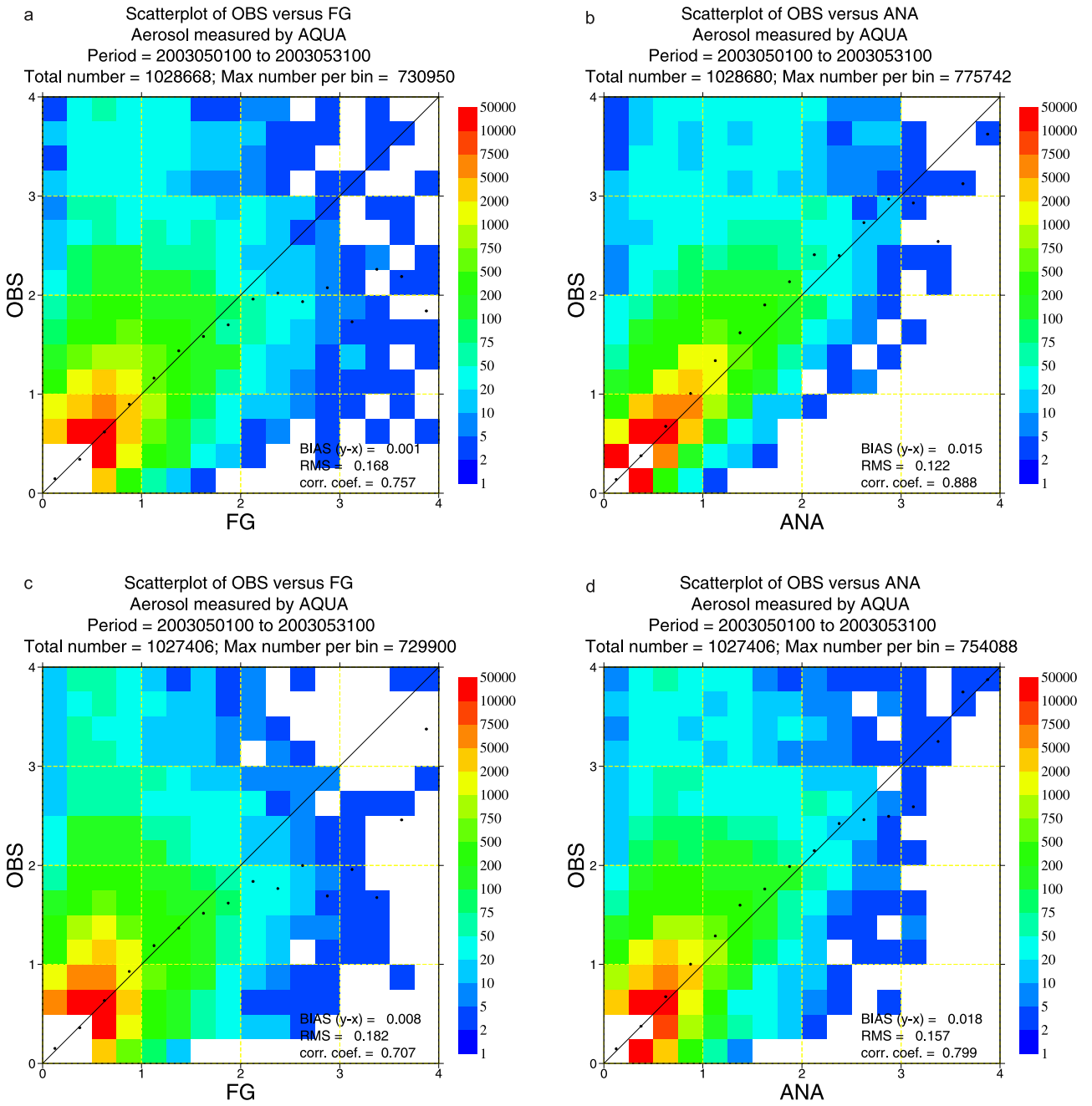

Figure 1. Scatterplots of MODIS Aqua observations of aerosol optical depth versus (a) first-guess optical depth and (b) analysis optical depth for the standard reanalysis run for May 2003. (c) Same as in Figure 1a and (d) same as in Figure 1b but using a logarithmic total aerosol mixing ratio variable in the control vector. See text for explanations. Note that the scatterplots only include MODIS data from the Aqua satellite, whereas data from the Terra satellite were also included in the assimilation.

tions versus first guess (Figure 1a) and analysis (Figure 1b). By visual inspection, it is apparent that the scatter in the analysis is smaller than in the first guess. The root mean square error with respect to the MODIS data is lower for the analysis (0.122) than for the first guess (0.168) while the correlation coefficient is higher for the analysis (0.888) than for the first guess (0.757), indicating a good performance of the analysis. However, while we did not expect the analysis to improve on the first-guess biases, it was surprising to notice that the analysis effectively has a larger bias than the first guess. The distribution appears to be skewed and it is evident from the shape of the scatterplot that the analysis is more efficient in increasing low values of optical depth than in reducing high values.

[36] This "asymmetric" behavior of the analysis merits further attention. As a first step we checked whether this bias could be caused by the choice of control variable presented in section 2.5. By definition this variable cannot be negative. However, in areas where the first guess is larger than the observed values, the minimization can produce negative analysis increments. When these negative increments are added to the trajectory values of total aerosol

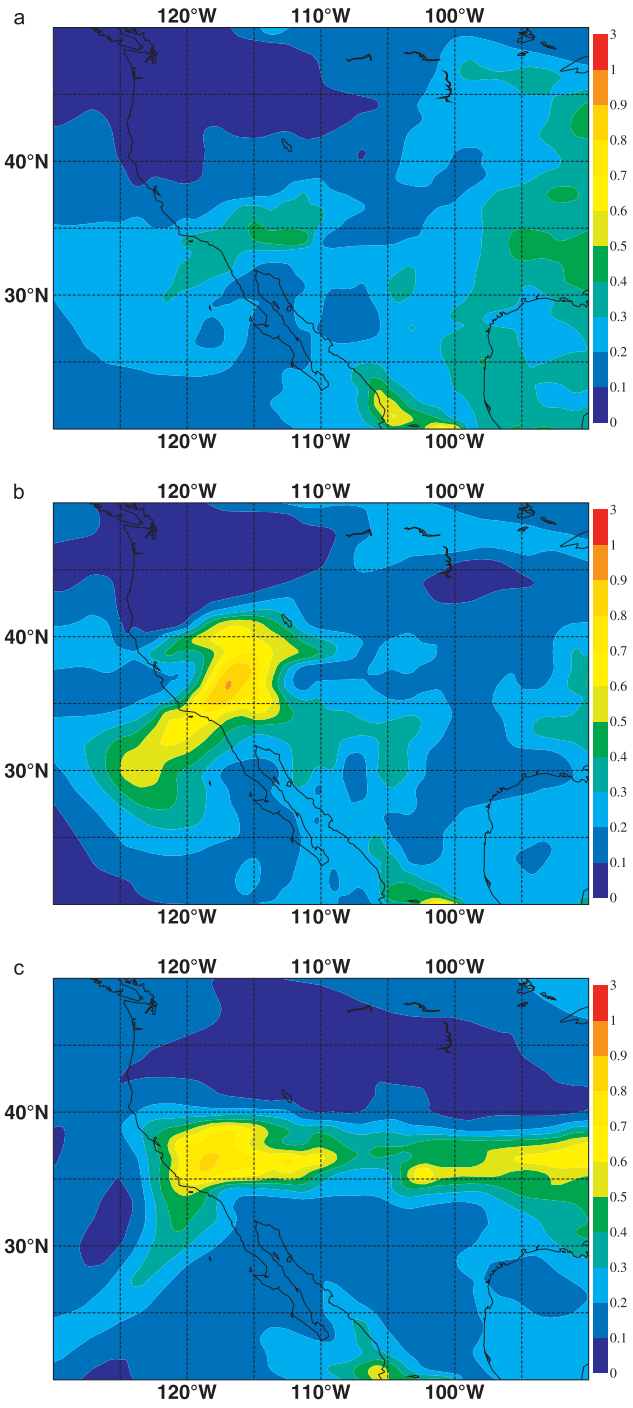

Figure 2. Comparisons of simulated aerosol optical depths for 11 July 2008 over California: (a) forecast from a free-running simulation valid at 0600 UTC, (b) forecast from the analysis using MODIS data valid at 0600 UTC, and (c) forecast from the analysis using MODIS data valid at 0000 UTC on 14 July 2008.

mixing ratio, it is possible that the updated value of mixing ratio becomes negative, and hence unphysical. In the implementation, this is avoided by resetting to zero all negative values of total aerosol mixing ratio. However, this could introduce a bias in the analysis. To further investigate this, a logarithmic total aerosol mixing ratio was implemented as control variable. By construction, this alternative control variable is positive definite and there is no need to reset the analysis total concentration to zero a posteriori. Figures 1c and 1d show scatterplots for an experiment with the logarithmic total aerosol mixing ratio. We can notice that in this case, the distribution of the points along the 1:1 line is more symmetric. The bias in the analysis is comparable to the first guess (0.018 versus 0.008) while the RMS is still lower (0.157 for the analysis versus 0.182 for the first guess) and the correlation coefficient is higher (0.799 versus 0.707). There is still, however, a tendency of the analysis to be more effective at increasing low values than decreasing large values.

[37] This behavior can be further explained by looking back at the error assumptions for the MODIS optical depths discussed in section 3.3. From the error formulations of equations (6) and (7) it appears that high values of optical depths are penalized more, since the error is prescribed as a percentage of the optical depth, implying that in an absolute sense high optical depths are assigned a larger error than low optical depths. In the minimization this translates to giving a lower "weight" to large (observed) values of AOD with respect to the background AOD, and, as a result, the model AOD is not changed much from its original value by insertion of observations.

[38] One possible solution is to implement a capping of the errors on the observations above a certain optical depth threshold, hence giving more weight to these observations. This will be considered in future reruns of the analysis along with more stringent quality checks and screening of the ingested data, following *Zhang et al.* [2008].

[39] As a side note, the implementation of the logarithmic variable did not dramatically improve the analysis performance. On the contrary, the RMS is higher and the correlation lower in the analysis with the logarithmic control variable than in the analysis with total mass mixing ratio. The reason for this could lie in the fact that the logarithmic control variable is only used at the level of the minimization, whereas the rest of the model is formulated in terms of mass mixing ratio. A more effective way to handle tracers could be to formulate the whole forward model in terms of logarithmic (hence positive definite) variables. This however would involve an extensive effort in modifying and rewriting the model, and it is not a viable option at this point. The use of alternative normalized control variables with a more Gaussian error distribution can still be investigated for future developments, following existing examples [*Hólm et al.*, 2002].

5. Impact of MODIS Data on the Aerosol Forecast

[40] Another measure of the success of the analysis is provided by the retention time of the information contained in the observations. By looking at the difference between forecasts from a free-running experiment with no assimilation of aerosol data and from the analysis in the near-real-time configuration we found that the system has a good memory after insertion of data. The impact is evident up to approximately 49–72 h. This is especially true in areas where an unusually large aerosol mass is injected into the atmosphere (e.g., California fires of summer 2008). Figure 2 shows the forecast of aerosol optical depth at

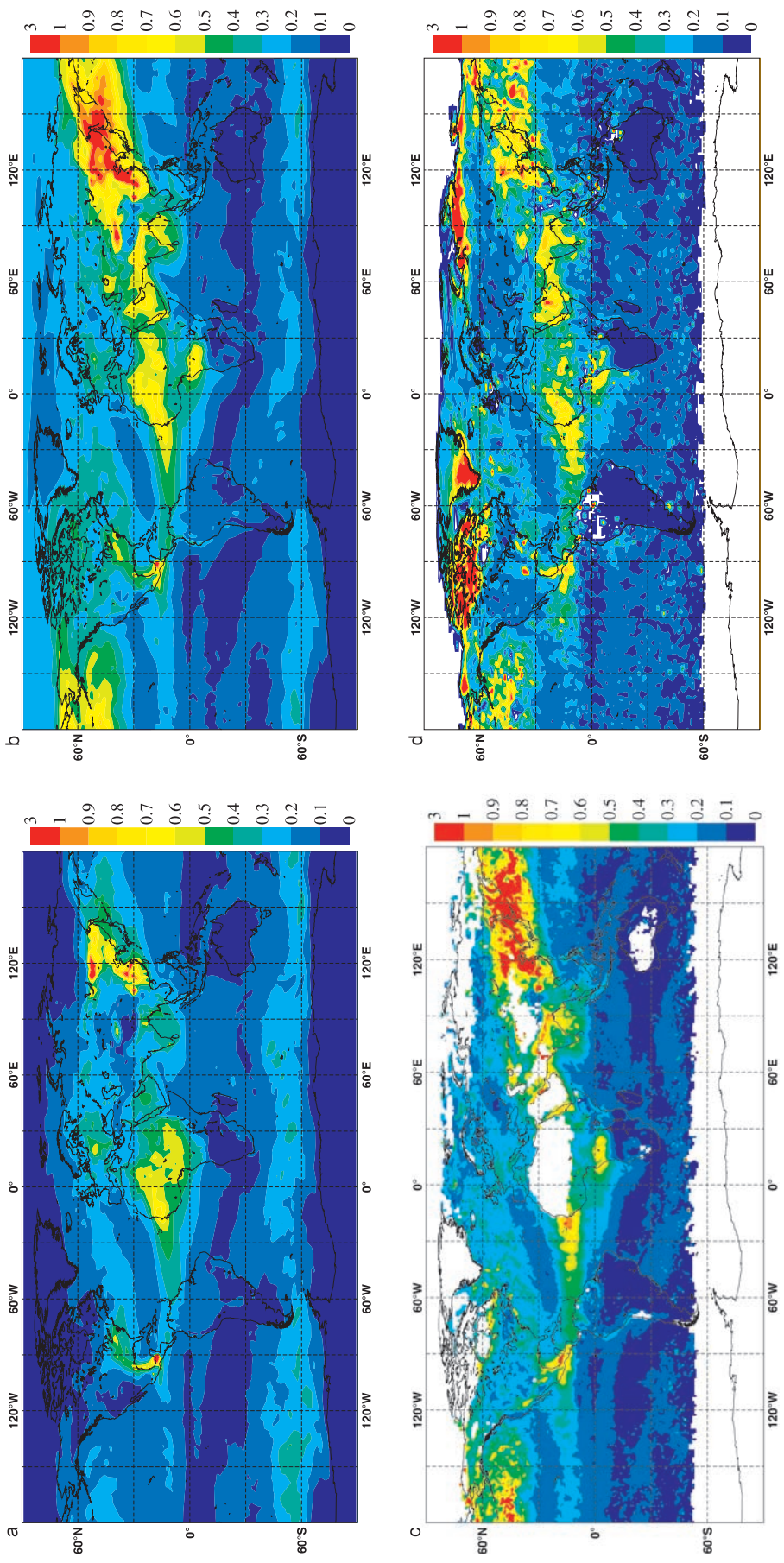

Figure 3. Comparisons of simulated aerosol optical depths from the new aerosol module implemented in the IFS model: (a) free-running forecast, (b) analysis using MODIS collection 5 observations, (c) MODIS AQUA, and (d) MISR aerosol optical depth for May 2003. The high values of AOD over Greenland, and other northern high-latitude areas in the MISR data plot, should be disregarded.

0600 UTC on 11 July 2008 for the California area from the free-running model and from the analysis using MODIS data. The position of the local peak in aerosol optical depth in the forecast produced from the analysis is north of Sacramento (38.43°N, 121.67°W), consistently with satellite observations of smoke produced by wildfires in the area. A similar peak in aerosol optical depth is completely lacking in the free-running simulation. Figure 2c shows the aerosol optical depth forecast valid for 0000 UTC 14 July 2008. The impact of the insertion of MODIS data is still evident after 72 h. After that timeframe the model relaxes to its "natural" state since the emission sources are not updated in the analysis. In a full assimilation system which would include a surface analysis, the retention time would probably be longer.

6. Reanalysis Results

[41] In this section we assess the performance of the long reanalysis by comparing it with other optical depth databases, both from spaceborne sensors (i.e., the Multiangle Imaging SpectroRadiometer, MISR) and from established ground-based Sun photometer networks (AERONET). Comparisons with MODIS data from the Aqua satellite are also shown for reference. A more in-depth validation of the analysis, which includes both optical depth and physical property data (aerosol mass concentration), will be presented in part 3.

6.1. Comparisons With MODIS and MISR Data

[42] The MISR instrument [*Diner et al.*, 1998, 2005] measures 4 bands (blue, green, red and near-infrared) at different viewing angles (0.0, 26.1, 45.6, 60.0, and 70.5 degrees) using nine cameras. The swath width is approximately 360 km. The global coverage time is 9 days, with repeat coverage between 2 and 9 days depending on latitude. Its unique viewing geometry allows MISR to measure aerosol optical depth over different reflecting surfaces including bright surfaces as deserts. The aerosol optical depth product is quoted to have an accuracy of 20% or 0.05 (whichever is larger) with greater accuracy over dark surfaces [*Kahn et al.*, 2007]. Although MISR retrievals cannot be assumed as "ground truth," since they suffer from inaccuracies related to cloud contamination, wind-speed assumptions, etc., they offer an independent data set with which assess the forecast and the analysis.

[43] Figure 3 compares between the free-running forecast of aerosol optical depth without any assimilation of aerosol data, the analysis of optical depth from assimilated MODIS observations, and the MISR aerosol optical depth for May 2003. MODIS AODs are also shown as reference. Optical depth retrievals are assimilated over both land and ocean. The model aerosol optical depths are averages of 3-hourly forecasts started at 00UTC from the free-running model and from the analysis. Figure 4 shows differences between the MODIS and MISR monthly means with respect to the forecast and analysis optical depths. Despite some evident discrepancies, Figures 3 and 4 show that the analysis is effective in bringing the model aerosol optical depth closer to the observations, especially in areas where the free-running forecast underestimates the AOD.

[44] The assimilation generally improves the aerosol distribution over areas with extensive biomass burning in equatorial West Africa. The aerosol amount in the Southern Ocean is lower in the analysis than in the free-running forecast, and is also in better agreement with the observations. Other areas, such as the Indian Ocean, the Indian subcontinent and Eastern Asia, are also improved. These areas are dominated by anthropogenic emissions and are not captured as well in the free-running simulation because of inadequate definition of the sources for these emissions. Note, however, the overall skill of the forecast model in predicting the global distribution of the aerosol fields, and thus providing a good first guess for the analysis. Of note is also the overall large positive bias of the analysis over Eurasia, and the inability of the analysis to constrain areas of large optical depths which are evident in the free-running forecast but absent in the observations (e.g., eastern United States). The possible reasons for this behavior have already been discussed in section 4. It is, however, instructive to see the geographical distribution of this bias to pinpoint in which areas the analysis can be improved both through the use of observations with better coverage and of higher quality and through refinements in the methodology.

[45] Figures 3 and 4 also highlight discrepancies between the two satellite products which can be as large as the largest departures in the free-running model and in the analysis.

6.2. Comparisons With AERONET Observations

[46] The AERONET program [*Holben et al.*, 1998] is a federation of ground-based remote sensing instruments providing globally distributed observations of spectral aerosol optical depth, inversion products, and precipitable water in diverse aerosol regimes. The aerosol optical depth data used in this comparison are the Level 2.0 (cloud-screened and quality-assured) product.

[47] Figure 5 shows some comparisons with AERONET independent data for the month of May 2003. In order to calculate a bias and a root mean square error (RMS) that are roughly indicative of global performance, data from a selected group of approximately evenly spaced, high-availability AERONET stations was used. The site selection was made using an algorithm which looped through all available sites, checking each for proximity to others. If two sites were found within 700 km of each other, then the site with greater availability (measured as the number of 6-h periods with at least one observation at 500 nm during January 2003) was kept and the other discarded. This resulted in a selection of 41 stations.

[48] The AODs from the model are averages over 6 h, whereas the AERONET observations are instantaneous. To make them comparable, the AERONET observations are averaged over the same period. Because the observations are unevenly spaced in time, a weighted mean is computed in such a way that it is equal to the mean of the series of straight lines that join neighboring observations over the period. Forecast AODs from the free-running experiment and the analysis are bilinearly interpolated to the observation location in space.

[49] The analysis is shown in red and the free-running forecast in blue in Figure 5. Both plots show that the

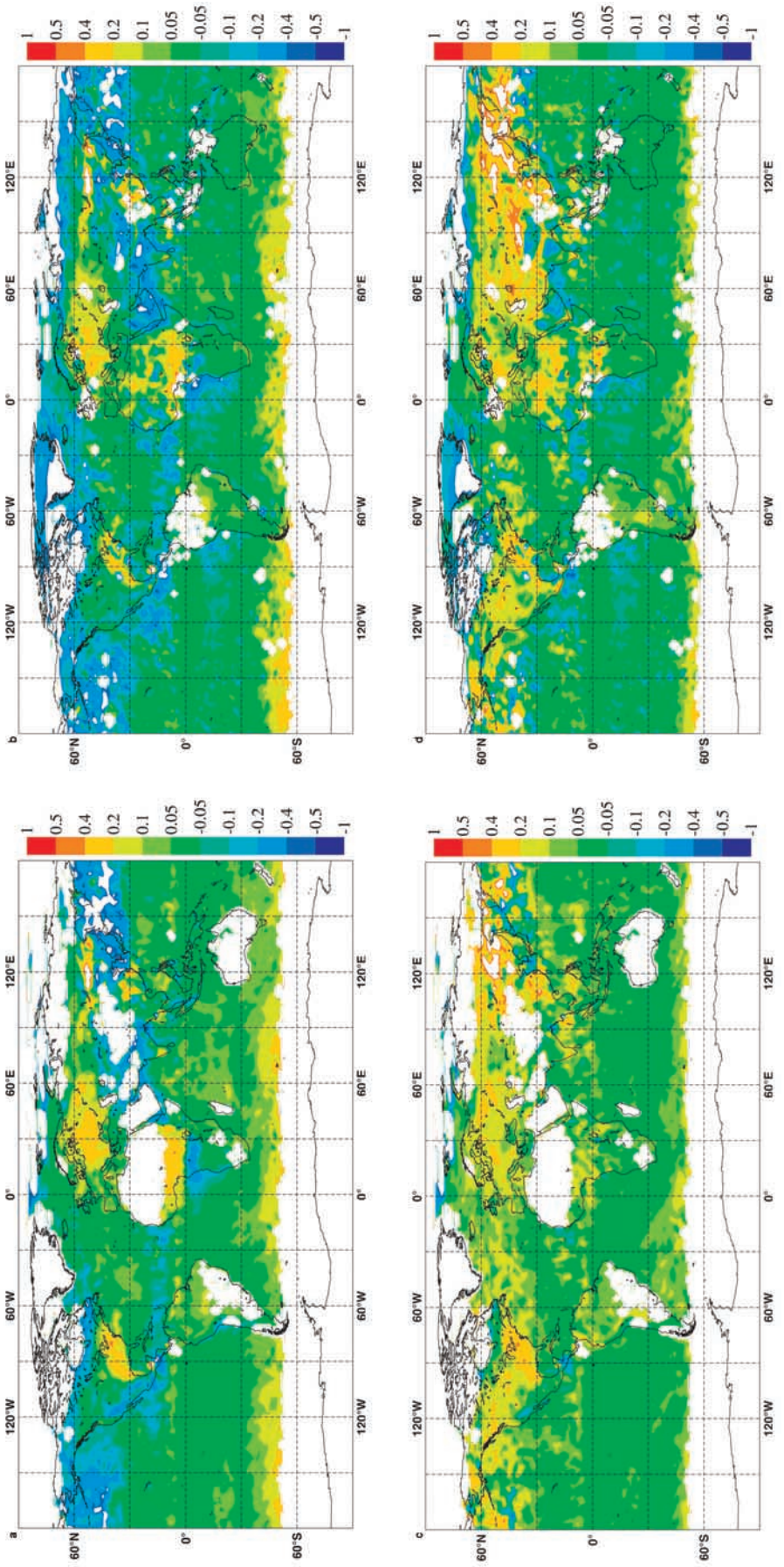

Figure 4. Global maps of AOD differences for May 2003: (a) free-running forecast minus MODIS Aqua observations, (b) free-running forecast minus MISR observations, (c) analysis minus MODIS Aqua observations, and (d) analysis minus MISR observations.

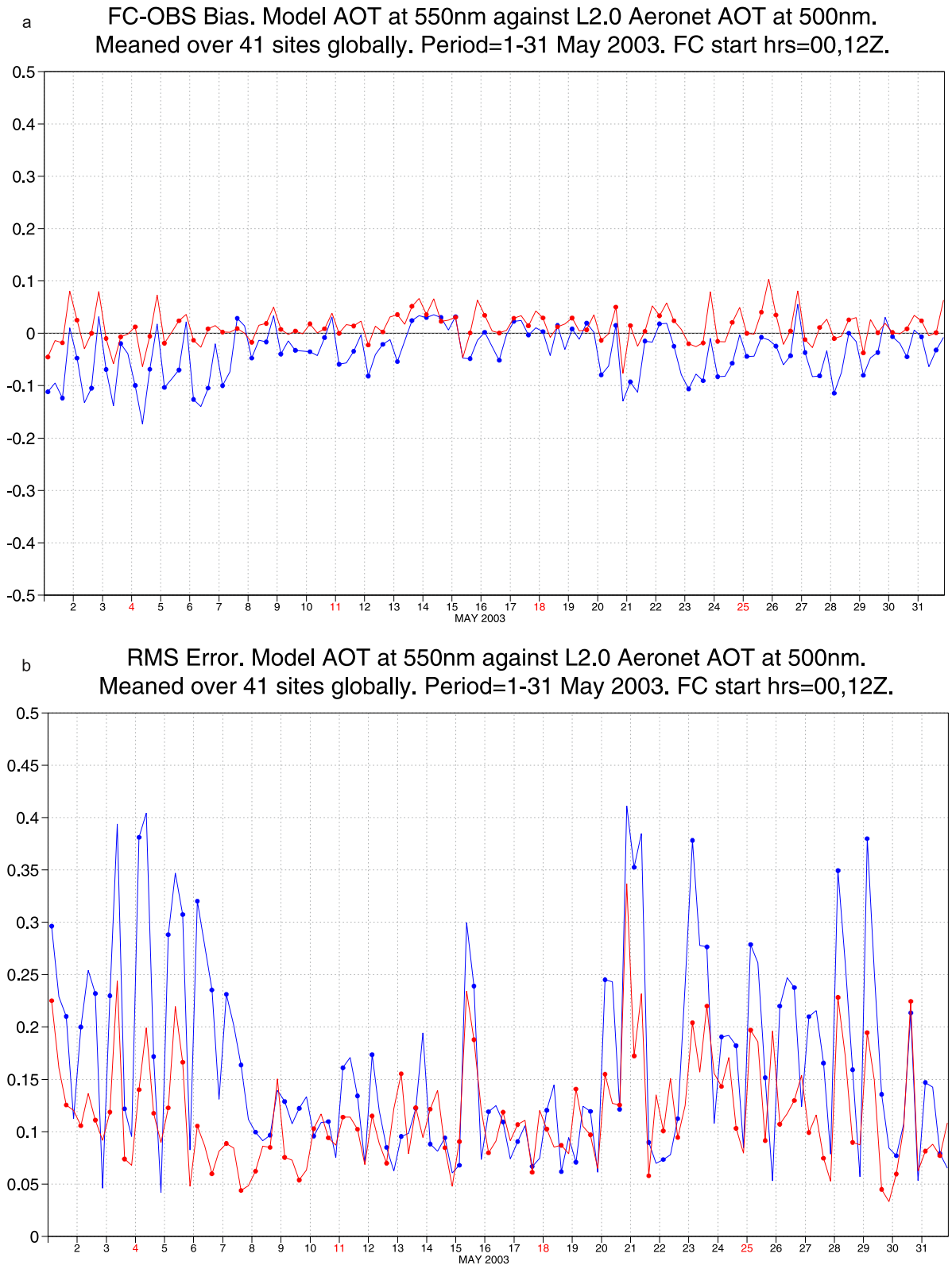

Figure 5. (a) Bias and (b) RMS of the AOD at 550 nm from the free-running forecast (blue) and analysis (red) with respect to AERONET ground-based observations at 500 nm for May 2003.

analysis is on average closer to the AERONET observations displaying a lower bias and RMS error than the forecast.

[50] As an additional example, Figure 6 compares the analyzed optical depth at 550 nm with the observed aerosol optical depth over the AERONET sites of Dakhla (Morocco), Solar Village (Saudi Arabia) and Fresno (California, USA). The contributions to the total optical depth from the single constituents are also shown. Note how over the sites of Dakhla and Solar Village, the analysis is able to reproduce the observed variability and intensity of the dust episodes, despite the lack of MODIS data which are not available over highly reflective surfaces.

6.3. A Saharan Dust Outbreak

[51] To further assess the performance of the analysis we looked at a case study relative to a major Saharan dust storm recorded in early March 2004. Cold air was advected from Europe to Western Africa, fanning out across the Sahara, highly diverging over subtropical regions and thus creating the dust storm. In the following days, the dust was blown out across the Atlantic Ocean and reached the coast of South America. The storm was detected by several satellite sensors and ground-based sites. Very large values of AOD were recorded. Figure 7 shows comparisons between AODs from the free-running model and the analysis compared to MODIS observations for 5–6 March 2004. The shape of the dust outflow is well represented in both free-running model and analysis, but the magnitude of the AODs is much larger in the latter in better agreement with the observations. This is also confirmed by looking at the AERONET data at key stations (see Figure 8). Figure 8 shows a comparison between AOD at 670 nm from the analysis and the free-running forecast and AERONET AODs at 675 nm for Agoufou (Mali), Dakar (Senegal) and Cape Verde. The peaks shown in the AERONET data are well captured by the analysis, with the exception of the 8–9 March AOD maximum over Agoufou. Level 2.0 AERONET data were used when possible. For the Agoufou station only level 1.5 data were available for the dates of interest. The plots in Figure 8 show again a good degree of skill of the analysis in representing the observed values of aerosol optical depth. Details on this and other case studies will be presented in part 3.

7. Conclusions and Future Outlook

[52] This study presented the general architecture and the first results of the GEMS aerosol assimilation system developed at ECMWF. The aerosol species active in the model are sea salt, desert dust, organic matter, black carbon and sulphate. Appropriate parameterizations and inventories are used to describe emission of these species. Aerosol physical processes such as sedimentation and wet/dry deposition are also included. The assimilation uses the operational 4D-Var apparatus which has been extended to include atmospheric tracers among the control variables. At present, the total mixing ratio is used as control variable for the aerosol assimilation. Increments in this variable are redistributed into the different species according to their fractional contributions. The background error statistics have been computed for the total aerosol mixing ratio using six months of aerosol forecast differences at 48 and 24 h (NMC method). The background error covariance matrix derived from this set of statistics has proven adequate to describe the error characteristics of the background aerosol fields, provided it is updated each time major model changes are implemented. The assimilation system uses retrievals of optical depth from the MODIS sensor on the Aqua and Terra satellites. All available observations over land (except bright surfaces) and ocean are used at their time and location over the 12-h 4D-Var window.

[53] Results from the reanalysis for 2003 show that the analysis is able to draw to the assimilated observations, although the analysis is more efficient in increasing rather than reducing the values of aerosol optical depth. The impact on the subsequent forecast of aerosol optical depth is felt up to 72 h after the insertion of data in the system. Comparisons with independent measurements of AOD from the ground-based AERONET network show that the analysis has a lower bias and a lower RMS for most sites than a free-running forecast without assimilation. For the month of May 2003 an average over 41 sites of the differences between AERONET AOD and the model AOD showed that the mean bias for the analysis is 0.012 while for the free-running forecast it is −0.036. The RMS is 0.117 for the analysis and 0.164 for the free-running forecast. Of particular note is the ability of the analysis to improve the AOD forecast over sites where the MODIS observations are not available. This occurs thanks to the influence of observations in the neighboring areas and to the spreading out of information in the horizontal and vertical directions due to the use of the dynamical model in the 4D-Var minimization.

[54] To make the analysis more effective, it will be necessary to assimilate other observations, for example AODs from the Spinning Enhanced Visible and Infrared Imager (SEVIRI) on board of the Meteosat Second Generation satellites (Meteosat-8 onward). Use of other sensors will also be investigated. MODIS retrievals also provide general information on the breakdown between fine and coarse particle optical depth. One possibility is to assimilate this information directly into the 4D-Var system. Another possibility is to make use of the Angstrom parameter which also gives information on the size of the aerosol particulate from observations of optical depth at different wavelengths. This will require a rethinking of the control variable and the possible introduction of more aerosol-related variables in the control vector.

[55] A third possibility, which will be given priority, is direct assimilation of multiwavelength reflectances. This development is already under way and the radiative transfer code for visible wavelengths has been already prepared to be incorporated into the IFS. The tangent linear and adjoint operators for the radiative transfer code (6S [*Vermote et al.*, 1997a, 1997b]), necessary for the incremental variational assimilation, are under development.

[56] The GEMS aerosol reanalysis for 2003–2004 was completed in July 2008. An in-depth review of the results and comparisons with yet more independent data sets is needed for a final assessment of the quality of the analysis. This will involve several of the partners in the GEMS project and will be presented in part 3. First results are however encouraging and show the capability of the analysis to provide good initial conditions for improved fore-

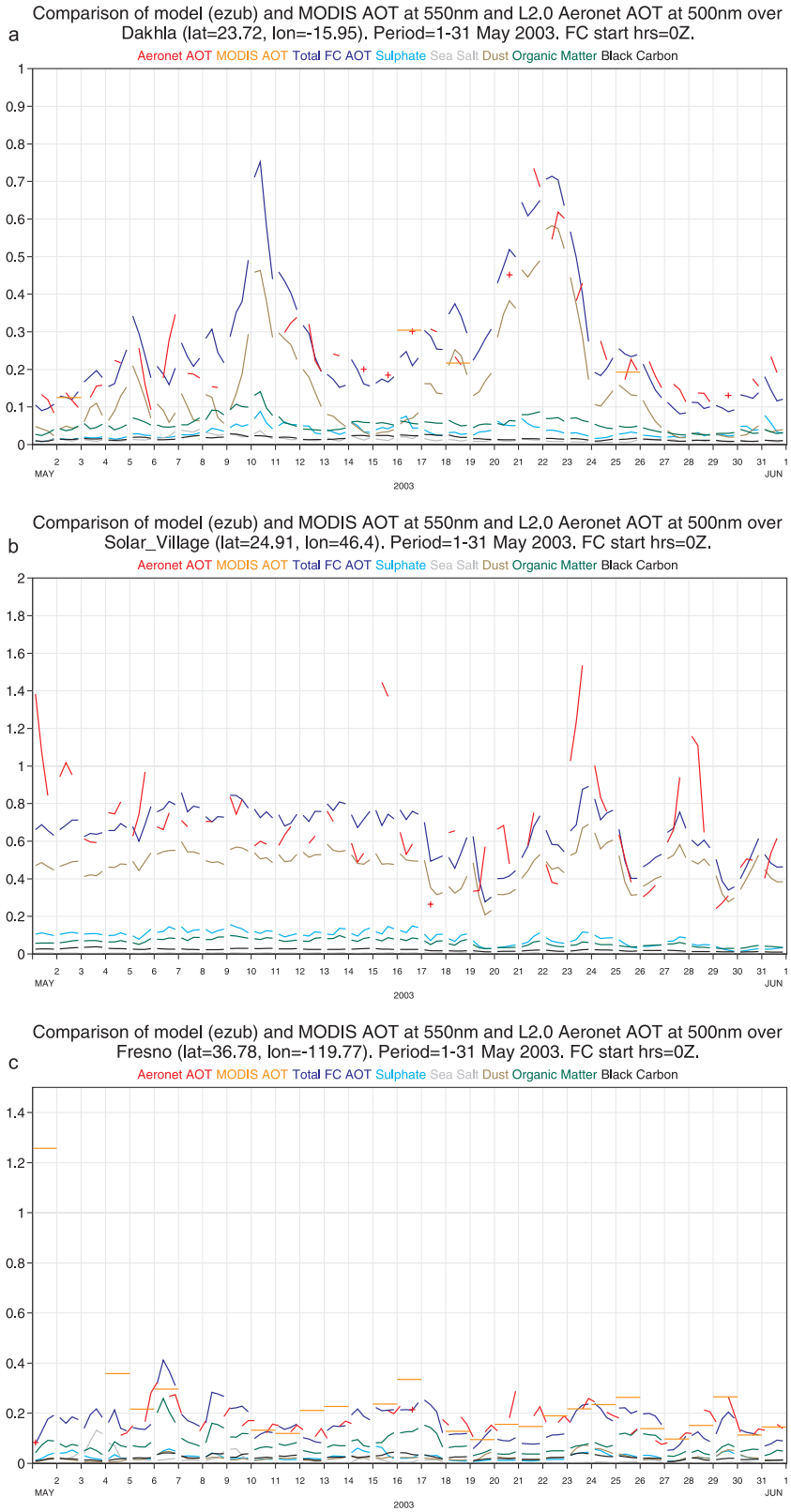

Figure 6. Comparisons of analysis aerosol optical depths with AERONET observations: (a) Dakhla (Morocco), (b) Solar Village (Saudi Arabia), and (c) Fresno (California). Color codes are as follows: red, AERONET AOD; purple, model total AOD; dark yellow, MODIS AOD; light blue, sulphate AOD; grey, sea salt AOD; light brown, dust AOD; green, organic matter AOD; and black, black carbon AOD.

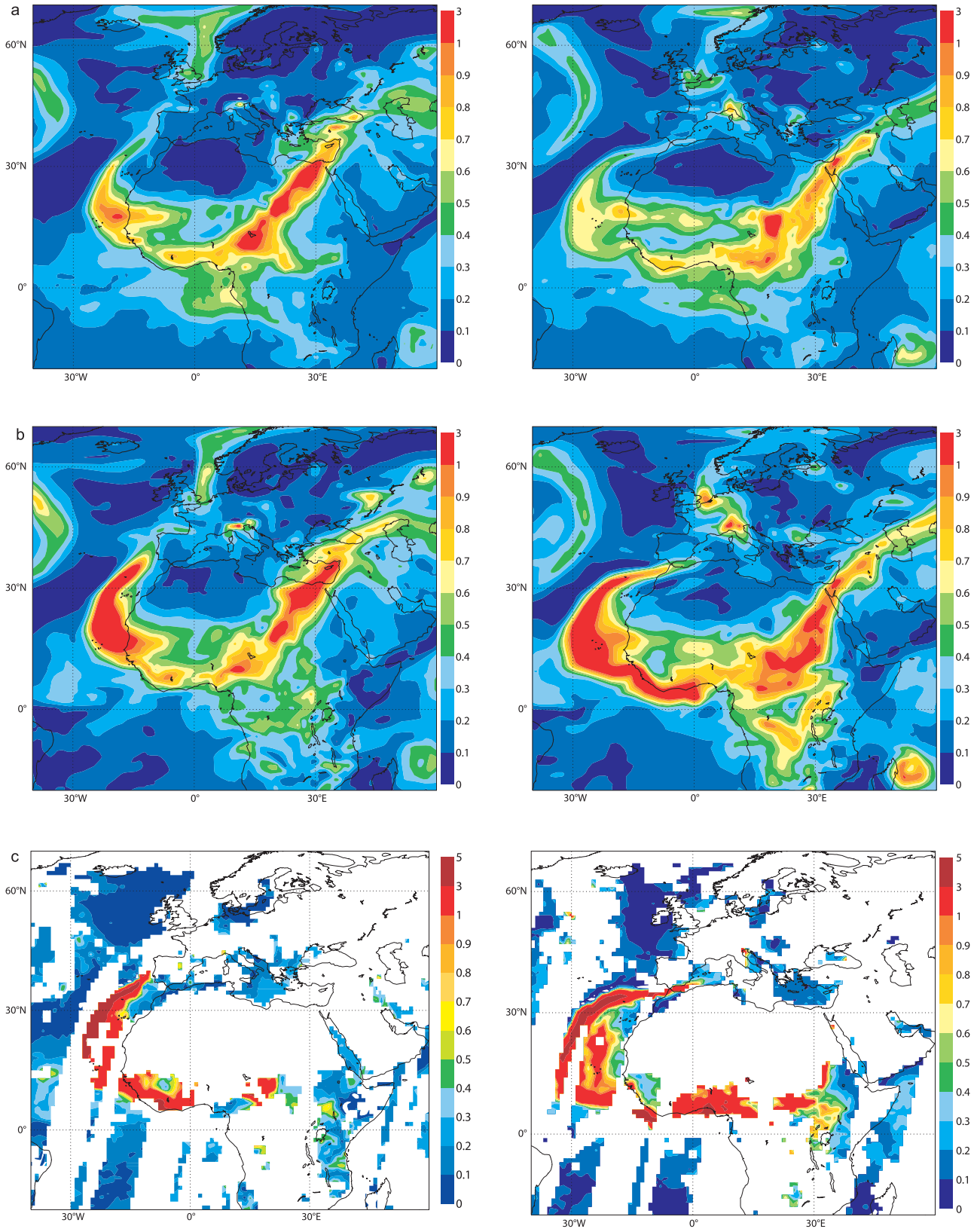

Figure 7. March 2004 Saharan dust outbreak: comparisons of free-running model and analysis 550 nm AODs with MODIS (assimilated) observations: (a) free running model, (b) analysis, and (c) MODIS observations for (left) 5 March 2004 at 1200 UTC and (right) 6 March 2004 at 1200 UTC.

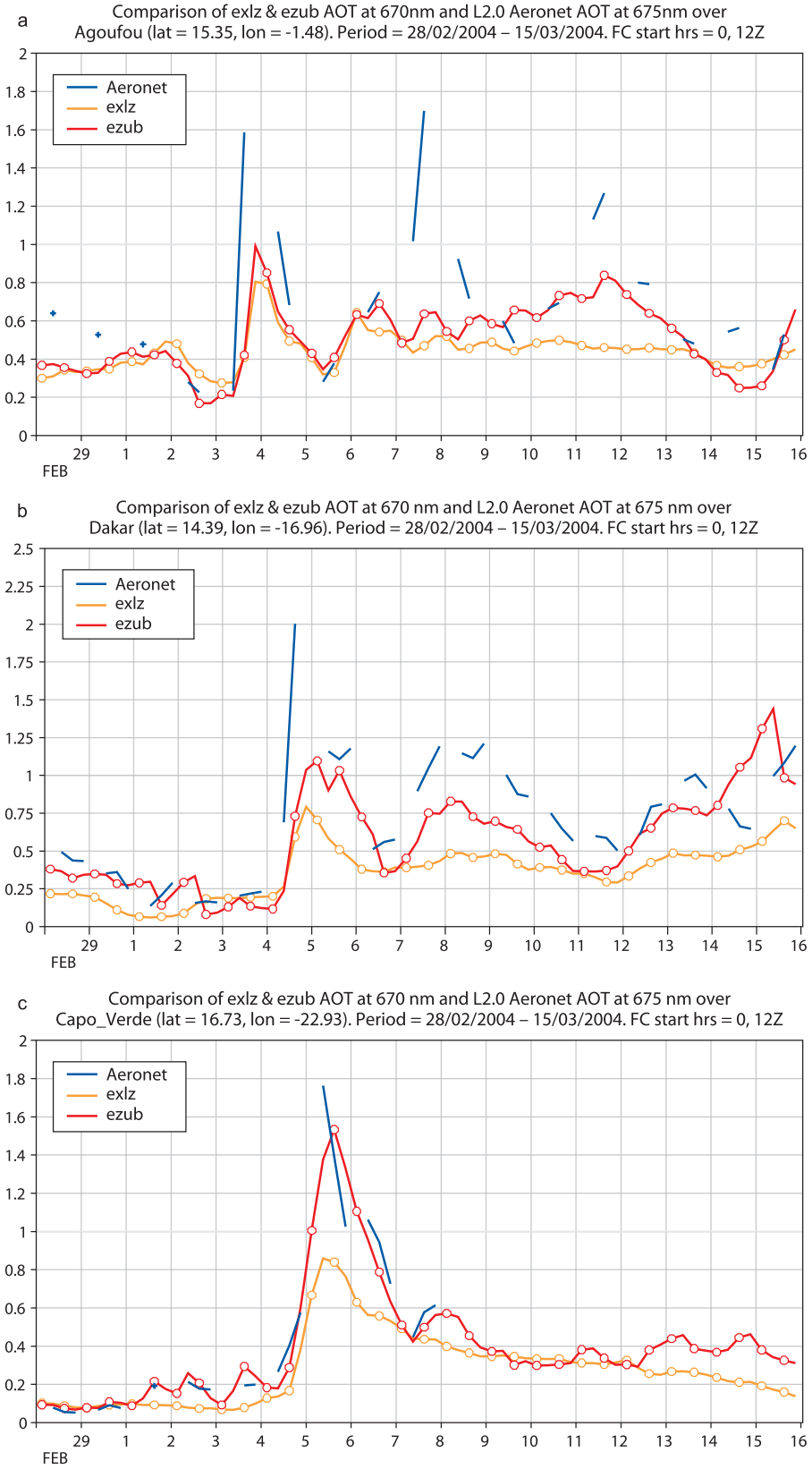

Figure 8. Comparisons of analysis aerosol optical depth at 675 nm with AERONET observations for the Saharan dust outbreak of March 2004: (a) Agoufou (Mali), (b) Dakar (Senegal), and (c) Cape Verde. AERONET data are shown in light blue, the analysis is in red, and the free-running forecast is in dark yellow.

casts of atmospheric aerosol fields. A follow-on project, the Monitoring Atmospheric Composition and Climate (MACC) project, also funded by the European Commission, will explore the feasibility of preoperational implementation of the GEMS assimilation system for reanalysis and real-time forecasts of aerosols. In MACC, there are also plans to make the aerosol fully interactive with the radiation scheme thus allowing us to explore fully the impact of the improved aerosol fields on the whole atmospheric system.

[57] **Acknowledgments.** This work is largely the result of a team effort, and the whole GEMS-AER team is wholeheartedly acknowledged. We gratefully acknowledge the developers of the GES-DISC (Goddard Earth Sciences Data and Information Services Center) Interactive Online Visualization and Analysis Infrastructure for providing an invaluable service of visualization and data processing for the MODIS and MISR data (see http://g0dup05u.ecs.nasa.gov/Giovanni/). AERONET data were obtained from the AERONET web site (http://aeronet.gsfc.nasa.gov/). The two anonymous reviewers of the manuscript are also thanked for their insightful and often challenging comments which helped improved on the original version of the paper. Thanks also go to Vinicio B. Korch for his support. GEMS is funded by the European Commission under the EU Sixth Research Framework Programme, contract SIP4-CT-2004-516099.

References

Bellouin, N., A. Jones, J. Haywood, and S. A. Christopher (2008), Updated estimate of aerosol direct radiative forcing from satellite observations and comparison against the Hadley Centre climate model, *J. Geophys. Res.*, *113*, D10205, doi:10.1029/2007JD009385.

Benedetti, A., and M. Fisher (2007), Background error statistics for aerosols, *Q. J. R. Meteorol. Soc.*, *133*, 391–405.

Benedetti, A., and M. Janisková (2008), Assimilation of MODIS cloud optical depths in the ECMWF model, *Mon. Weather Rev.*, *136*, 1727–1746.

Benedetti, A., et al. (2008), Aerosol analysis and forecast in the ECMWF integrated forecast system: Data assimilation, *Tech. Memo. 571*, Eur. Cent. for Medium-Range Weather Forecasts, Reading, U. K.

Boucher, O., M. Pham, and C. Venkataraman (2002), Simulation of the atmospheric sulfur cycle in the LMD GCM: Model description, model evaluation, and global and European budgets, *Note 23*, 26 pp., Inst. Pierre-Simon Laplace, Paris, France. (Available at http://www.ipsl.jussieu.fr/poles/Modelisation/NotesSciences.htm)

Collins, W. D., P. J. Rasch, B. E. Eaton, B. V. Khattatov, and J.-F. Lamarque (2001), Simulating aerosols using a chemical transport model with assimilation of satellite aerosol retrievals: Methodology for INDOEX, *J. Geophys. Res.*, *106*, 7313–7336.

Courtier, P., J.-N. Thépaut, and A. Hollingsworth (1994), A strategy for operational implementation of 4D-Var, using an incremental approach, *Q. J. R. Meteorol. Soc.*, *120*, 1367–1387.

Dee, D. P. (2005), Bias and data assimilation, *Q. J. R. Meteorol. Soc.*, *131*, 3323–3343.

Diner, D. J., et al. (1998), Multi-angle Imaging Spectroradiometer (MISR) description and experiment overview, *IEEE Trans. Geosci. Remote Sens.*, *36*, 1072–1087.

Diner, D. J., et al. (2005), The value of multiangle measurements for retrieving structurally and radiatively consistent properties of clouds, aerosols, and surfaces, *Remote Sens. Environ.*, *97*, 495–518.

Errera, Q., and D. Fonteyn (2001), Four-dimensional variational chemical assimilation of CRISTA stratospheric measurements, *Mon. Weather Rev.*, *102*, 12,253–12,265.

Fisher, M. (2006), Wavelet" J_b—A new way to model the statistics of background errors, *ECMWF Newsl.*, *106*, 23–28.

Fonteyn, D., Q. Errera, M. De Maziére, G. Franssens, and D. Fussen (2000), 4D-Var assimilation of stratospheric aerosol satellite data, *Adv. Space Res.*, *26*, 2049–2052.

Generoso, S., F.-M. Bréon, F. Chevallier, Y. Balkanski, M. Schulz, and I. Bey (2007), Assimilation of POLDER aerosol optical thickness into the LMDz–INCA model: Implications for the Arctic aerosol burden, *J. Geophys. Res.*, *112*, D02311, doi:10.1029/2005JD006954.

Holben, B. N., et al. (1998), AERONET: A federated instrument network and data archive for aerosol characterization, *Remote Sens. Environ.*, *66*, 1–16.

Hollingsworth, A., et al. (2008), The Global Earth-system Monitoring using Satellite and in-situ data (GEMS) Project: Towards a monitoring and forecasting system for atmospheric composition, *Bull. Am. Meteorol. Soc.*, *89*, 1147–1164, doi:10.1175/2008BAMS2355.1.

Hólm, E., E. Andersson, A. Beljaars, P. Lopez, J.-F. Mahfouf, A. J. Simmons, and J.-N. Thépaut (2002), Assimilation and modelling of the hydrological cycle: ECMWF's status and plans, *Tech. Memo. 383*, 55 pp., Eur. Cent. for Medium-Range Weather Forecasts, Reading, U. K.

Kahn, R. A., M. J. Garay, D. L. Nelson, K. K. Yau, M. A. Bull, B. J. Gaitley, J. V. Martonchik, and R. C. Levy (2007), Satellite-derived aerosol optical depth over dark water from MISR and MODIS: Comparisons with AERONET and implications for climatological studies, *J. Geophys. Res.*, *112*, D18205, doi:10.1029/2006JD008175.

Kahnert, M. (2008), Variational data analysis of aerosol species in a regional CTM: Background error covariance constraint and aerosol optical observation operators, *Tellus, Ser. B*, *60*, 753–770, doi:10.1111/j.1600-0889.2008.00377.

Lewtas, J. (2007), Air pollution combustion emissions: Characterization of causative agents and mechanisms associated with cancer, reproductive, and cardiovascular effects, *Mutat. Res. Rev. Mutat. Res.*, *636*, 95–133.

Lopez, P., and E. Moreau (2005), A convection scheme for data assimilation: Description and initial tests, *Q. J. R. Meteorol. Soc.*, *131*, 409–436.

Morcrette, J.-J., et al. (2008), Aerosol analysis and forecast in the European Centre for Medium-Range Weather Forecast Integrated Forecast System: 1. Forward modeling, *J. Geophys. Res.*, *114*, D06206, doi:10.1029/2008JD011235.

Niu, T., S. L. Gong, G. F. Zhu, H. L. Liu, X. Q. Hu, C. H. Zhou, and Y. Q. Wang (2008), Data assimilation of dust aerosol observations for the CUACE/dust forecasting system, *Atmos. Chem. Phys.*, *8*, 3473–3482.

Parrish, D. F., and J. C. Derber (1992), The National Meteorological Center's spectral statistical-interpolation analysis system, *Mon. Weather Rev.*, *120*, 1747–1763.

Rasch, P. J., W. D. Collins, and B. E. Eaton (2001), Understanding the Indian Ocean Experiment (INDOEX) aerosol distributions with an aerosol assimilation, *J. Geophys. Res.*, *106*, 7337–7355.

Reddy, M. S., O. Boucher, N. Bellouin, M. Schulz, Y. Balkanski, J.-L. Dufresne, and M. Pham (2005), Estimates of global multicomponent aerosol optical depth and direct radiative perturbation in the Laboratoire de Météorologie Dynamique General Circulation Model, *J. Geophys. Res.*, *110*, D10S16, doi:10.1029/2004JD004757.

Remer, L. A., et al. (2005), The MODIS aerosol algorithm, products and validation, *J. Atmos. Sci.*, *62*, 947–973.

Thompson, M. C., A. M. Molesworth, M. H. Djingarey, K. R. Yameogo, F. Belanger, and L. E. Cuevas (2006), Potential of environmental models to predict meningitis epidemics in Africa, *Trop. Med. Int. Health*, *11*, 781–788.

Tompkins, A. M. (2005), A revised cloud scheme to reduce the sensitivity to vertical resolution, *Tech. Memo. 0599*, 25 pp., Res. Dep., Eur. Cent. for Medium-Range Weather Forecasts, Reading, U. K.

Tompkins, A. M., and M. Janisková (2004), A cloud scheme for data assimilation: Description and initial tests, *Q. J. R. Meteorol. Soc.*, *130*, 2495–2517.

Trémolet, Y. (2005), Incremental 4D-Var convergence study, *Tech. Memo. 469*, 34 pp., Eur. Cent. for Medium-Range Weather Forecasts, Reading, U. K.

Tsigaridis, K., Y. Balkanski, M. Schulz, and A. Benedetti (2008), Global error maps of aerosol optical properties: An error propagation analysis, *Atmos. Chem. Phys. Discuss.*, *8*, 16,027–16,059. (Available at www.atmos-chem-phys-discuss.net/8/16027/2008/)

Vermote, E. D., D. Tanré, J. L. Deuzé, M. Herman, and J.-J. Morcrette (1997a), Second simulation of the satellite signal in the solar spectrum: An overview, *IEEE Trans. Geosci. Remote Sens.*, *35*, 675–686.

Vermote, E. D., D. Tanré, J. L. Deuzé, M. Herman, and J.-J. Morcrette (1997b), Second simulation of the satellite signal in the solar spectrum (6S): An overview, 6S User guide, version 2, report, 53 pp., Tex. A&M Univ., College Station.

Weaver, C., A. da Silva, M. Chin, P. Ginoux, O. Dubovik, D. Flittner, A. Zia, L. Remer, B. Holben, and W. Gregg (2007), Direct insertion of MODIS radiances in a global aerosol transport model, *J. Atmos. Sci.*, *64*, 808–826.

Zhang, J., and J. S. Reid (2006), MODIS aerosol product analysis for data assimilation: Assessment of over-ocean level 2 aerosol optical thickness retrievals, *J. Geophys. Res.*, *111*, D22207, doi:10.1029/2005JD006898.

Zhang, J., J. S. Reid, D. L. Westphal, N. L. Baker, and E. J. Hyer (2008), A system for operational aerosol optical depth assimilation over global oceans, *J. Geophys. Res.*, *113*, D10208, doi:10.1029/2007JD009065.

A. Benedetti, A. Dethof, R. J. Engelen, M. Fisher, J. W. Kaiser, L. Jones, J.-J. Morcrette, M. Razinger, A. J. Simmons, and M. Suttie, European Centre for Medium-Range Weather Forecasts, Shinfield Park, Reading RG2 9AX, UK. (angela.benedetti@ecmwf.int)

O. Boucher, Met Office, Hadley Centre, FitzRoy Road, Exeter EX1 3PB, UK.

H. Flentje, Meteorologisches Observatorium Hohenpeissenberg, Deutscher Wetterdienst, Albin-Schwaiger-Weg 10, D-82383 Hohenpeissenberg, Germany.

N. Huneeus, Laboratoire des Sciences du Climat et de l'Environnement, L'Orme des Merisiers, Bat. 712, Point Courrier 132, F-91191 Gif-sur-Yvette, France.

S. Kinne, Max-Planck-Institut für Meteorologie, Bundestrasse 53, D-20146 Hamburg, Germany.

A. Mangold, Observations Department, Royal Meteorological Institute of Belgium, B-1180 Uccle, Belgium.